Time-resolved x-ray microdiffraction studies of phase transformations during rapidly propagating reactions in Al/Ni and Zr/Ni multilayer foils

J. C. Trenkle,[1] L. J. Koerner,[2] M. W. Tate,[2] Noël Walker,[1] S. M. Gruner,[3] T. P. Weihs,[1] and T. C. Hufnagel[1,a)]
[1]*Department of Materials Science and Engineering, Johns Hopkins University, Baltimore, Maryland 21218-2681, USA*
[2]*Department of Physics, Cornell University, Ithaca, New York 14853, USA*
[3]*Department of Physics, Cornell High Energy Synchrotron Source, Cornell University, Ithaca, New York 14853, USA*

(Received 17 January 2010; accepted 15 April 2010; published online 2 June 2010)

We showed how intermetallic formation reactions can be studied under rapid heating (10^6–10^7 K s^{-1}) using x-ray microdiffraction with temporal resolution on microsecond time scales. Rapid heating was achieved by initiating an exothermic reaction in multilayer foils comprising alternating nanoscale layers of elemental metals. The reaction occurred in a front ~100 μm wide which propagated across the foil at ~1–10 m s^{-1}. By using synchrotron x-rays focused to a small spot (60 μm diameter) and a fast pixel-array detector, we were able to track the evolution of phases in the reaction front during the initial heating transient, which occurred in approximately 1 ms, through cooling over a period of hundreds of milliseconds. In Al/Ni multilayer foils, the first phases to form were an Al-rich liquid and the cubic intermetallic AlNi (which likely formed by nucleation from the liquid). In foils of overall composition AlNi, this is the stable intermetallic and the only phase to form. In foils of composition Al_3Ni_2, during cooling we observed a peritectic reaction between AlNi and the remaining liquid to form Al_3Ni_2, which is the stable phase at room temperature and the final product of the reaction. This is in contrast to the sequence of phases under slow heating, where we observed formation of nonequilibrium Al_9N_2 first and do not observe formation of a liquid phase or the AlNi intermetallic. We also observed formation of an amorphous phase (along with crystalline ZrNi) during rapid heating of Zr/Ni multilayers, but in this system the temperature of the reaction front never reached the lowest liquidus temperature on the Zr–Ni phase diagram. This implies that the amorphous phase we observed was not a liquid arising from melting of a crystalline phase. We suggest instead that a Zr-rich amorphous solid formed due to solid-state interdiffusion, which then transformed to a supercooled liquid when the temperature exceeded the glass transition temperature. Formation of the supercooled liquid presumably facilitated continued rapid intermixing, which may be necessary to sustain a self-propagating reaction front in this system. © *2010 American Institute of Physics*. [doi:10.1063/1.3428471]

I. INTRODUCTION

An understanding of diffusion and phase transformations is central to successful processing of many materials. In particular, with the advent of layered thin film technologies there has been great interest in how these processes occur over small length scales in the presence of steep concentration gradients. For instance, it is known that nucleation rates and growth mechanisms for compound formation reactions in thin films often differ from those in bulk samples where concentration gradients are more gradual.[1] Most of these thin film studies have involved either isothermal annealing or only moderate heating rates (~1 K s^{-1}). But at higher heating rates, the time available for diffusion, nucleation, and growth of both stable and metastable phases is limited, resulting in different phase formation sequences and microstructures.

One way to achieve rapid heating under controlled conditions is by initiating a self-propagating exothermic reaction in a nanoscale multilayer foil.[2–8] In such a foil, constituents with large negative heats of mixing are deposited in alternating nanoscale layers. Because the diffusion distances are small, once initiated the reaction front can propagate rapidly and reach temperatures in excess of 1500 K in less than one millisecond, for an effective heating rate of 10^6–10^7 K s^{-1}. The reaction characteristics, including peak temperature and velocity, can be precisely controlled by tailoring the multilayer structure (e.g., the individual layer thicknesses) during deposition or by subsequent annealing.[9,10]

Studying phase transformations that occur under these conditions requires a combination of spatial resolution on the order of 100 μm (the approximate width of the reaction front) and temporal resolution of approximately 100 μs (the time for the reaction front to pass a fixed point in the material). Recently, we have shown that this is possible with x-ray diffraction using a highly intense, focused synchrotron x-ray beam, and an area x-ray detector capable of short exposure times and with the ability to capture several frames in rapid succession.[11] In that paper, we presented preliminary results

a)Author to whom correspondence should be addressed. Electronic mail: hufnagel@jhu.edu.

on Al/Ni multilayers of overall nominal composition Al_3Ni_2; here we provide additional details on that system as well as new results on multilayers of nominal composition AlNi and $Zr_{55}Ni_{45}$. For both Al/Ni compositions, we observe the formation of an Al-rich liquid and the cubic intermetallic phase AlNi in the earliest stages of the reaction. In the Zr/Ni multilayers, we also observe early formation of an amorphous phase, but in this case the heat released by the reaction is insufficient to cause melting. We propose that the amorphous phase we observe is the result of a solid-state reaction at the Zr/Ni interfaces, with subsequent heating causing the interfacial layer to transform to a supercooled liquid when the temperature exceeds the glass transition temperature of the amorphous alloy.

II. BACKGROUND

In bulk diffusion couples, growth of compound phases is diffusion limited and in principle all of the equilibrium phases should be able to form. It has long been known, however, that in nanoscale diffusion couples this is not necessarily the case; frequently, metastable phases form (as in solid-state amorphization, for instance) or one or more equilibrium phases are not observed. A variety of models have been proposed to explain and predict phase formation sequences (including formation of metastable phases) during solid-state transformations in nanoscale systems. For instance, Gösele and Tu[12] suggested that for slow heating of thin films, where diffusion is not limiting, interfacial reaction barriers may cause one (or more) of the equilibrium phases to be absent. In their model, it is assumed that all possible phases can nucleate, and whether a given phase is observed experimentally depends on whether it grows (or shrinks) under the given conditions.

Thompson pointed out, however, that interdiffusion is required to form critical-size nucleii of the product phases; thus, nucleation is controlled not only by the factors influencing the barriers to nucleation (such as the interfacial free energies) but by diffusion rates.[13] He was able to show that solid-state amorphization is to be expected in systems with a large diffusional asymmetry between the two elements. Perhaps the best-known example of this is in Ni–Zr multilayers, in which an amorphous interlayer grows between layers of crystalline Ni and Zr.[14,15] While the growth rate of the amorphous layer is controlled by diffusion, the maximum thickness is determined by the heterogeneous nucleation of a crystalline intermetallic compound at the interfaces between the amorphous Ni–Zr and the crystalline Zr.[16] Thus, the maximum thickness of the amorphous layers decreases with increasing reaction temperature because higher temperatures facilitate nucleation of the competing crystalline intermetallic phases.

Besides these primarily kinetic arguments, several authors have suggested that steep concentration gradients can impede nucleation of otherwise stable phases for thermodynamic reasons.[17–20] The basic argument is that a thin layer of metastable solid solution (either crystalline or amorphous) at the interface will necessarily contain a steep concentration gradient, which reduces the driving force for nucleation of a compound phase and thus increases the activation barrier for nucleation. Hodaj and Gusak[20] enumerated several possible modes of nucleation in a steep concentration gradient, with the dominant mode being determined by both thermodynamic and kinetic parameters. In most cases, nucleation of phases with wide stable ranges of composition is favored over phases with limited ranges of stability (e.g., line compounds). One might expect that the mode offering the lowest nucleation barrier would dominate, but the relative contribution of each mode also depends on the atomic mobilities in both the parent and product phases.[19,21]

An application of these ideas to Al/Ni multilayers is provided by the work of da Silva Bassani and co-workers, who showed that the first phase to form depended on both the bilayer period and the average composition of the multilayer.[22] In particular, with increasing bilayer period the composition of the first intermetallic phase to form moved away from the overall composition of the multilayers. Furthermore, they showed that the diffusion of Ni into Al (estimated as $x \approx \sqrt{Dt}$, where x is the diffusion distance, D is the diffusion rate, and t is time) was constant for both the onset and completion of the formation of the first intermetallic phase. These observations are consistent with the idea that the concentration gradient must be reduced below a critical level before nucleation of new intermetallic phases can occur.[23]

Most of this prior work, both theoretical and experimental, involved either isothermal conditions or low heating rates [$\sim 1\ \mathrm{K\ s^{-1}}$, typical of differential scanning calorimetry (DSC)]. But heating rate can have a profound influence on phase formation sequence, through its effect on interdiffusion and by limiting the time available for nucleation of new phases. Knowing this, researchers interested in self-propagating reactions (in powder compacts as well as multilayers) have sought to characterize the phases that form during rapid heating. One technique is to quench the propagating reaction and study the resulting phases *ex situ*, but is clear that at least in some cases this produces misleading results.[11] More promising is the use of *in situ* x-ray diffraction, which has been applied to the study of self-propagating reactions in powder compacts. For example, in Ni/Al compacts both Boldyrev and co-workers[24] and Wong and co-workers[25] observed an unidentified intermediate phase prior to the formation of cubic AlNi. We note, however, that *in situ* experiments on powder compacts are complicated by the heterogeneous structure of the material. This means that the observations may be sampling various stages of the reaction front as it propagates through the material. In comparison, the vapor-deposited multilayers studied here have a precisely layered structure that enables a uniform reaction front, which in turn allows investigation of each stage of the reaction. The consistency of the structure (combined with careful experimental technique) also enables direct comparison of results from several specimens, even in the earliest stages of the reaction where events are occurring on the microsecond time scale.

Another promising development is dynamic transmission electron microscopy (DTEM) with nanosecond resolution using a pulsed electron source, which has recently

TABLE I. Chemical and reaction characteristics of the foils used in this study.

Nominal composition (at. %)	Actual composition (at. %)	Bilayer period (nm)	Velocity ($m\ s^{-1}$)	Adiabatic reaction temperature (K)	Measured peak temperature (K)	Maximum heating rate($K\ s^{-1}$)	Maximum cooling rate ($K\ s^{-1}$)
Al_3Ni_2	$Al_{60}Ni_{37}V_3$	100	2.8 ± 0.2	1720	1650 ± 150	$\sim 10^6$	1.3×10^4
AlNi	$Al_{49}Ni_{47}V_4$	100	3.9 ± 0.2	1840	1760 ± 150	$\sim 10^7$	1.9×10^4
$Zr_{55}Ni_{45}$	$Zr_{53}Ni_{44}V_3$	75	0.4 ± 0.2	1225	1200 ± 150	$\sim 10^5$	8.6×10^3

been applied to the study of self-propagating reactions in Ni/Al multilayers.[26] This technique provides diffraction information similar to that of *in situ* x-ray diffraction, and adds the ability for time-resolved imaging on the nanosecond scale. For instance, Kim and co-workers[26] showed the development of a solid/liquid cellular structure at the leading edge of the propagating reaction front. However, DTEM requires thin specimens (~ 100 nm), and since thinner foils lose heat more rapidly to the environment care must be taken in comparing the TEM results to those from thicker foils (such as the ~ 30 μm specimens studied here). A more detailed comparison between the results of the two techniques is provided below.

III. EXPERIMENTAL

A. Reactive foils

For this work, we studied multilayer foils with nominal compositions of Al_3Ni_2, AlNi, and $Zr_{55}Ni_{45}$ (Table I). The sputtering targets were Ni–7 wt % V and either Al 1100 alloy or 99.8% pure Zr. (Adding vanadium to the nickel target renders it paramagnetic, facilitating sputter deposition of thick specimens.) The specimens therefore had actual overall compositions of $Al_{60}Ni_{37}V_3$, $Al_{49}Ni_{47}V_4$, and $Zr_{53}Ni_{44}V_3$ (all in atomic percent), but for simplicity we refer to them below by their nominal compositions. The entire binary phase diagrams for Al–Ni and Zr–Ni systems are reprinted in Fig. 1 for easy reference.

We deposited the multilayers by dc magnetron sputtering onto brass substrates, from which we subsequently removed them to produce free-standing foils. The total thickness of the foils was ~ 30 μm, chosen to maximize the signal in the x-ray diffraction experiments.

The bilayer period (the total thickness of two adjacent layers) was 100 nm for both Al/Ni multilayer systems and 75 nm for the Zr/Ni multilayers. The substrates were placed on a carousel which rotated the substrates past each sputtering gun in turn, with a source-to-substrate distance of 8.9 cm for all depositions. The chamber pressure prior to deposition was less than 10^{-6} torr, and the pressure of Ar during deposition was 1.0 mtorr for Al/Ni multilayers and 0.75 mtorr for Zr/Ni multilayers.

We measured the velocity and temperature-time profile for the self-propagating reactions in a separate set of experiments. The velocities were measured by sensing the light emitted by the reaction front as it passed a series of optical fibers coupled to a single photodetector. As the reaction front propagated past the fibers, the photodetector recorded a series of step increases in light level. By taking the time derivative of the photodetector signal we determined the time the front passed each fiber and, using the known separation of the fibers, calculated the velocity of the reaction front (Table I).

The temperature-time profiles for each foil composition were measured using a custom built two-color ratio pyrometer similar to that described in Ref. 27. Briefly, we positioned a fiber optic close to the foil to capture light emitted by the propagating reaction front. The optical signal was split into two paths, each of which was filtered to a (different) narrow range of wavelengths using dichroic filters and measured by a photodetector. By taking the ratio of these two signals, applying a suitable calibration, and correcting for the emissivities of the surface material,[28] we obtained temperature-time profiles. From this profile, we extracted the peak temperature, heating rate, and cooling rate for each foil

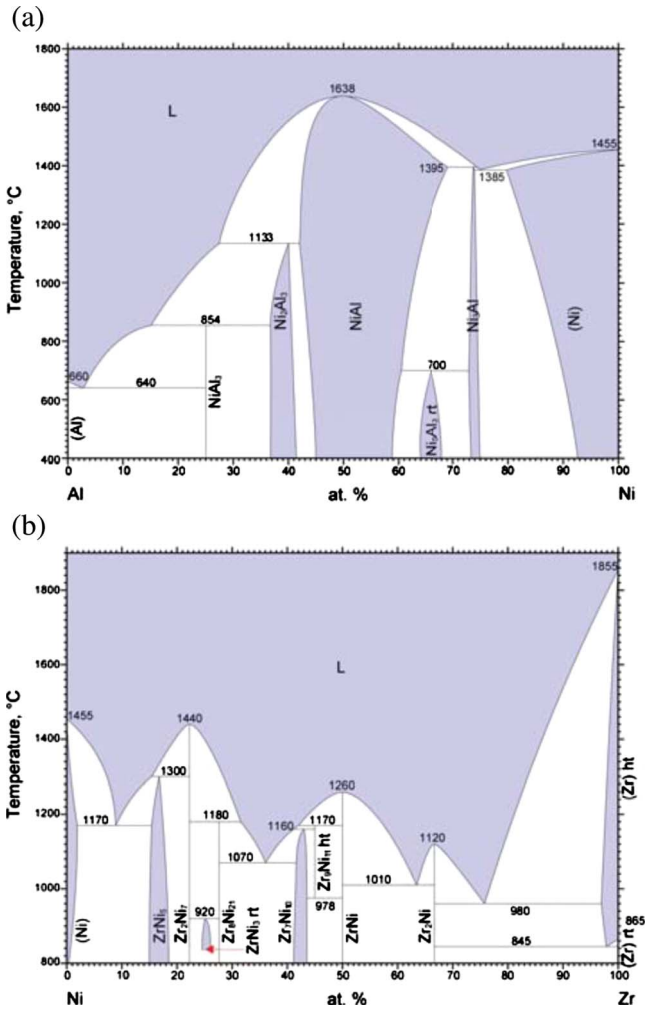

FIG. 1. (Color online) (a) Al–Ni and (b) Zr–Ni phase diagrams (Refs. 49 and 60).

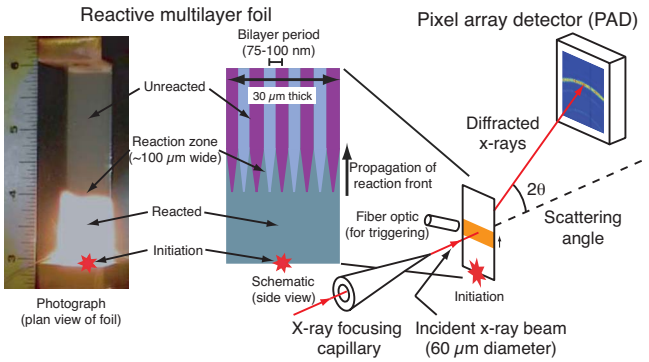

FIG. 2. (Color online) Schematic of the experimental configuration used to perform *in situ* x-ray diffraction on nanoscale reactive multilayers at CHESS. Also included is a schematic of the cross section of a reacting foil and a real-time photograph of a propagating reaction in plane view. The markers on the ruler in the photograph are inches. Reproduced from Ref. 11; used by permission.

(Table I). We also calculated the adiabatic reaction temperature based on the heat of reaction (measured by DSC) using a weighted average of the temperature-dependent elemental heat capacities and assuming that all phases were in the solid state.[9] For all foils, the measured peak reaction temperature agrees with the calculated adiabatic reaction temperature to within the uncertainty in the measurement (±150 K).

B. *In situ* x-ray microdiffraction

We performed microdiffraction experiments in transmission geometry on wiggler beam line A2 at the Cornell High Energy Synchrotron Source (CHESS) (Fig. 2). A sagittally focusing W/B_4C multilayer monochromator with a bandpass of 1.9% was used to select 8.2 keV (wavelength $\lambda=1.5$ Å) x-rays from the synchrotron beam.[29] This energy was chosen to avoid Ni fluorescence, minimize absorption in the specimen, and optimize detector efficiency (98% efficiency at the selected energy). The x-rays were focused to a 60 μm diameter spot using quartz capillary PEB605 placed 5.5 cm ahead of the specimen.[30] This experimental arrangement yielded approximately 1×10^{13} photons per second in the focused spot.

We recorded the diffracted x-rays with a pixel-array detector (PAD) consisting of a 100×92 array of 150 μm square pixels (1.50×1.38 cm overall) (Ref. 31) placed approximately 22 mm from the sample. We positioned the detector above the straight-through x-ray beam, centered on a scattering angle 2θ of approximately 45° with the detector surface normal to the scattered x-ray beam at that angle. In this position, the detector could record the diffracted intensity over a range of scattering vector magnitudes q ($=4\pi\sin\theta/\lambda$) from approximately 1.8 to 4 $Å^{-1}$ and captured ~15% of a complete diffraction ring.

Preliminary experiments showed that phase transformations occurred over times ranging from microseconds as the reaction front passed the x-ray beam to hundreds of milliseconds during cooling. Each pixel on the PAD has eight storage elements, allowing eight successive frames to be collected before readout. Since this was not enough to record microsecond-duration exposures over the entire course of the reaction, we repeated each experiment several times. The initial transient was recorded using exposure times of either 50 μs (for the Al/Ni foils) or 300 μs (for the Zr/Ni foils), with an additional interval of 5 μs between frames. These initial exposure times were determined by the velocity of the reaction front (Table I) and attenuation of the incident beam. The time it took the reaction front to cross the incident x-ray beam provided an upper limit while the intensity of the diffracted beam limited how short exposures could be.

For the much slower events that occur during cooling we introduced a delay between triggering of the detector (see below) and the start of data collection and increased the exposure time to 5 ms, with up to 45 ms between frames. Furthermore, to improve the signal-to-noise ratio (particularly for the shorter exposure times) we repeated each combination between two and six times, on nominally identical foils. The times were structured such that the last frame of the series from each foil overlapped (in time) with the first frame of the next series. This allowed us to ensure consistency of results from one series to the next and compile a complete sequence of the reaction events using data collected from multiple foils.

We initiated reactions in the foils in a localized spot by bringing an electrically charged metallic wire in contact with the grounded foil to create an electrical spark. Since each experiment was repeated several times, it was important to be able to trigger the detector at appropriate times with a reproducibility significantly better than the shortest exposures (50 μs). To do this we used an optical system consisting of an optical fiber, photodetector, and pulse height analyzer, which is described in more detail elsewhere.[28] Because the optical fiber sensed light from a region larger than the x-ray beam, the detector was triggered before the reaction front arrived at the x-ray beam. The interval between triggering of the detector and arrival of the reaction front at the beam depended on the reaction velocity (Table I) and was 180 μs for Al_3Ni_2, 100 μs for AlNi, and 1375 μs for $Zr_{55}Ni_{45}$ foils. To avoid ambiguity, in what follows we define time $t=0$ to be the time at which the detector was triggered, not the time at which the reaction front reached the x-ray beam. The two-dimensional diffraction patterns recorded by the detector were corrected for detector artifacts (as described in Ref. 28) and azimuthally integrated to produce the one-dimensional diffraction patterns (intensity $v\cdot q$) shown below.

IV. RESULTS AND DISCUSSION

In all three systems, we observed a similar general phase progression: the reactants were consumed as the reaction front approached the x-ray beam, and an amorphous phase and a crystalline intermetallic phase formed in <1 ms as the reaction front passed. We were not able to determine (given the temporal and spatial resolution of our measurements) which phase formed first, but for reasons discussed below we believe that the amorphous phase forms first in each case. These were the only phases observed until some 30–40 ms later when, during cooling, additional transformations occurred to produce the final microstructure. In each case, the

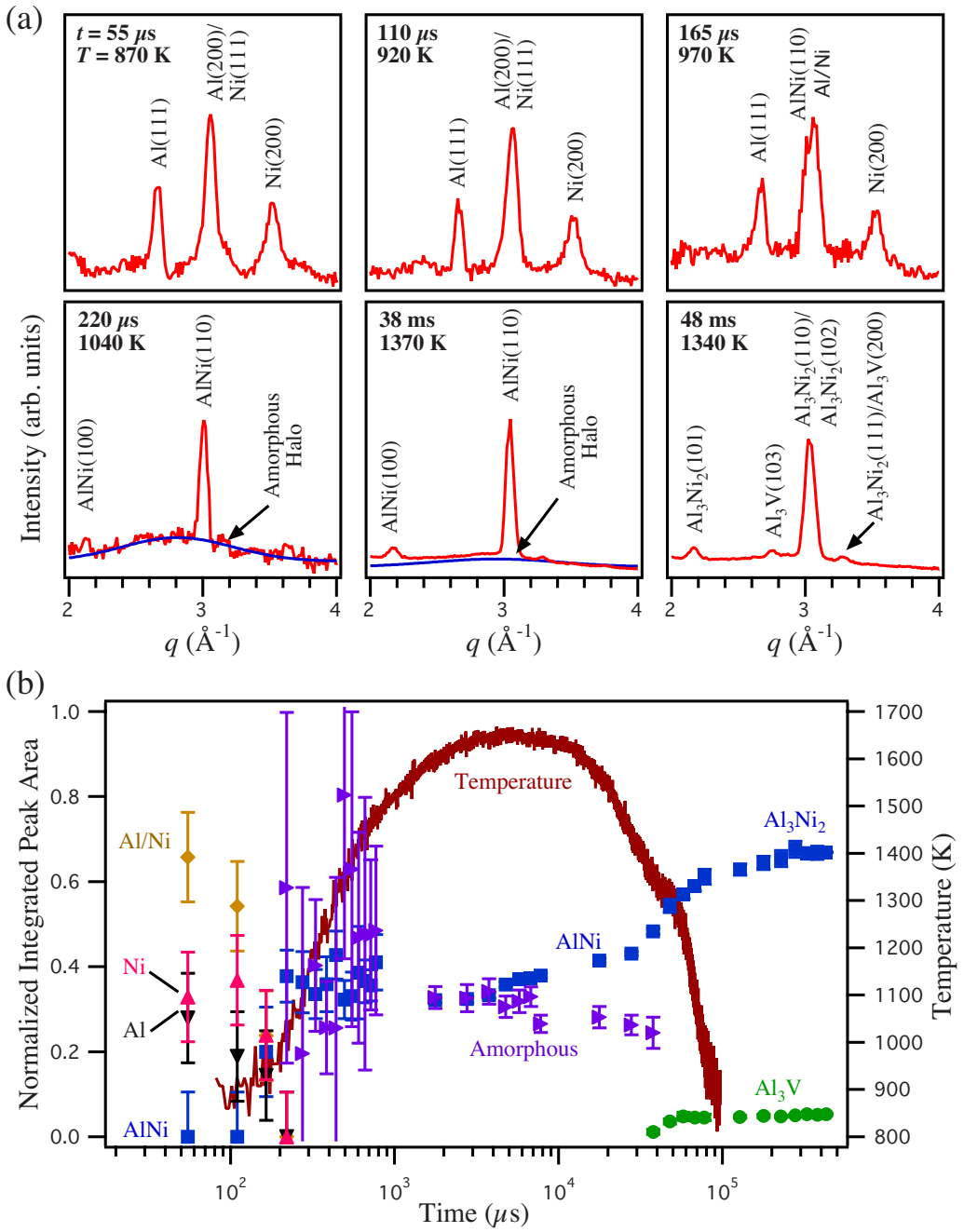

FIG. 3. (Color online) (a) Diffraction patterns of phase transformations during a self-propagating reaction in an Al_3Ni_2 foil. The blue line in patterns at $t = 220$ μs and 38 ms is a fit to the broad halo in the data which is attributed to the presence of an amorphous phase during this time range. (b) Integrated peak areas and temperature during the reaction (including cooling). Because the Al_3Ni_2 (110) and (102) peaks could not be resolved from one another and from the AlNi(110) peak, they are represented as one data series labeled "AlNi." The area is measured from the AlNi(110) peak and the Al_3Ni_2(110) and Al_3Ni_2(102) peaks (which cannot be differentiated spatially). (Adapted from Ref. 11.)

final phases were those predicted by the respective equilibrium phase diagrams, but the sequence of phase formation was different from that observed at slower heating rates.

A. Al_3Ni_2 foils

We have presented the results of the Al_3Ni_2 foils in a previous letter.[11] Here, we briefly review those results in order to make comparisons with the other two systems, and provide more detail and analysis. Representative diffraction patterns from various times during the course of the transformation sequence are shown in Fig. 3(a). Prior to the arrival of the reaction front at the x-ray spot ($t \leq 110$ μs), we observed only peaks from fcc Al and Ni. These are the distinct Al(111) and Ni(200) peaks, as well as a peak with overlapping contributions from Al(200) and Ni(111). At $t = 165$ μs (approximately the time that the reaction front arrived at the x-ray beam), we observe the formation of the cubic (B2 structure) intermetallic AlNi (as a shoulder on the Al(200)/Ni(111) peak) and the development of a broad scattering feature, which we attribute to melting of the Al layers to form a liquid. The pyrometry data indicate that at about this same time the temperature exceeded the melting point of pure Al (933 K). Furthermore, we determined that the liquid is Al-

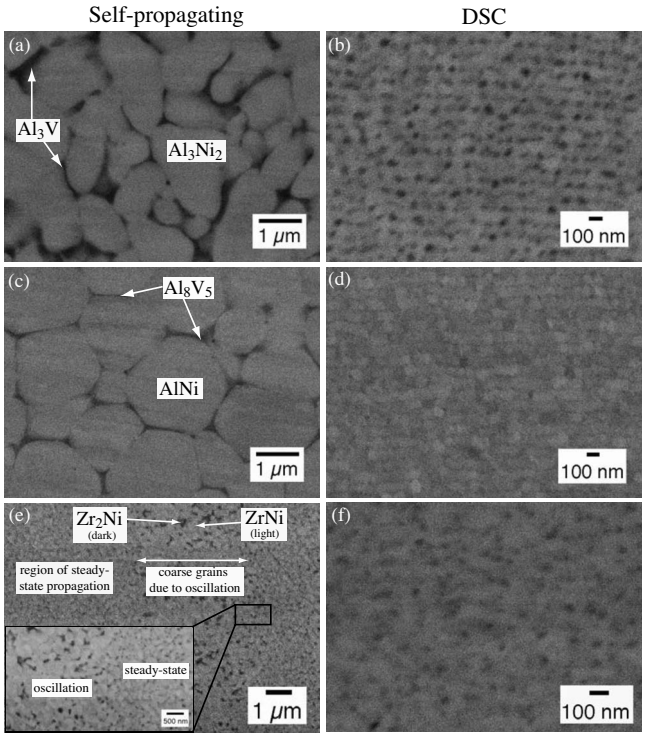

FIG. 4. Microstructures of Al_3Ni_2, AlNi, and Zr_2Ni foils after a (a,c,e) self-propagating reaction passed from left to right and (b,d,f) annealing (respectively) taken using back scattered scanning electron microscopy. The inset in (e) displays the coarse and fine-grained regions in the reacted Zr_2Ni foils. The duplex (coarse/fine) microstructure is discussed in Sec. IV C.

rich based on the q position of the broad scattering maxima ($\sim$2.9 Å^{-1}).[32–35] The apparent coexistence of fcc and liquid Al is likely due to the limited spatial resolution of the experiment; the x-ray beam was probably sampling both fcc Al ahead of the reaction front as well as liquid Al within it. By the next frame (55 μs later), the reaction front has passed the x-ray beam, all of the Al and Ni have been consumed, and only cubic AlNi and the amorphous phase remain.

The only other phase transformation we observed was the ternary peritectic reaction

$$\mathrm{AlNi} + L \rightarrow \mathrm{Al_3Ni_2} + \mathrm{Al_3V},$$

which occurred much later (30–40 ms after passage of the reaction front) during cooling. This ternary peritectic appears on the equilibrium Al–Ni–V phase diagram at 1373 K,[36] and an inflection point in the pyrometry signal occurs at this time at $\sim$1350 K. (The relatively rapid cooling rate of $\sim 1.4 \times 10^4$ K s^{-1} apparently results in some undercooling.) The general sequence of phase formation during the self-propagating reaction (neglecting the V-containing phases) is, therefore,

$$\mathrm{Al(fcc)} + \mathrm{Ni(fcc)} \rightarrow \mathrm{Al(liquid)} + \mathrm{AlNi} \rightarrow \mathrm{Al_3Ni_2}.$$

The final microstructure consists of Al_3Ni_2 and Al_3V, which are the equilibrium phases for the overall composition of these foils. A scanning electron micrograph of the final microstructures in cross section is shown in Fig. 4(a). The self-propagating reaction produces a coarse, equiaxial distribution of phases with no residual evidence of the original layered structure. This suggests that the microstructure at some point had a significant liquid fraction, consistent with our observation of an increasing background in the diffraction data.

To study the effect of heating rate, we reacted identical foils in a DSC heating them at 0.7 K s^{-1} and stopping the reaction at several points to determine which phases were present with *ex situ* x-ray diffraction. For these experiments, the phase formation sequence (again neglecting the V-containing phases) is quite different

$$\mathrm{Al(fcc)} + \mathrm{Ni(fcc)} \rightarrow \mathrm{Al_9Ni_2} + \mathrm{Al} + \mathrm{Ni} \rightarrow \mathrm{Al_3Ni} + \mathrm{Al} + \mathrm{Ni} \rightarrow \mathrm{Al_3Ni_2},$$

as reported earlier.[37] The microstructure of the foils reacted in the DSC is shown in Fig. 4(b). Even though the final phases are the same as in the foils that experienced the self-propagating reaction, the microstructure is markedly different—not only are the phases finer, but there is clear evidence of the original layering. Specifically, the phases appear periodically with $\sim$100 nm spacing, same as the bilayer period of the as-deposited foils. Presumably this is because the multilayer does not melt (even partially) during slow heating; instead, the developing phases form by nucleation (at high rates due to the high driving force at low temperatures) at pre-existing interfaces.

Similar phase sequences have been observed in other isothermal and low heating-rate experiments of Al/Ni multilayers with nominal overall compositions of AlNi and Al_3Ni_2.[23,38–46] Although the exact phase sequence differs from study to study (depending on the composition and bilayer period of the multilayers), in all cases intermediate phases (typically Al_9Ni_2 and Al_3Ni) are observed prior to the formation of the final (equilibrium) phases. As discussed above, there are a variety of models for predicting the phase formation sequence; for example Blobaum and co-workers[23] explained their observation of the formation of Al_9Ni_2 in light of the effect of composition gradients on nucleation.[19] They argued that steep concentration gradients make it impossible to form critical-size nuclei of competing phases, which have restricted compositional ranges of solubility. Although other interpretations are possible, a common feature of all isothermal or low heating-rate experiments is ample time for nucleation of new phases—the only question is which phase will form first.

In the case of a self-propagating reaction, the heating rate is much higher (10^5–10^7 K s^{-1}, Table I) and the multilayer exceeds the maximum temperature of stability of the Al-rich phases [1127 K for Al_3Ni and 1406 K for Al_3Ni_2 in Fig. 1(a)] in less than a millisecond (Fig. 3). The rapid heating has two effects. Kinetically, the time available for diffusion and nucleation is quite short. Thermodynamically, the driving force for nucleation of these phases (which, to first order, is proportional to the undercooling) is dropping as the temperature rises. Calculation of nucleation rates of these phases is difficult because of the strong dependence on unknown quantities, such as the interfacial free energies. Nevertheless, it seems apparent that rapid heating makes their formation more difficult.

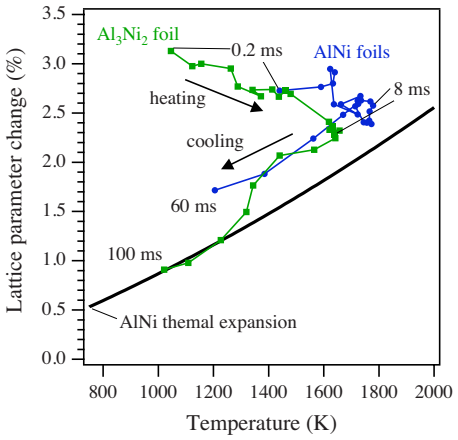

FIG. 5. (Color online) The change in the lattice spacing of AlNi (B2) phase as a function of temperature in the AlNi and Al_3Ni_2 foils. Points are labeled according to the time t of measurement; arrows indicating heating and cooling of the foils are also presented as a reference of time. The transformation in the Al_3Ni_2 foil from AlNi to Al_3Ni_2 is also indicated. For comparison, the calculated thermal expansion of bulk polycrystalline AlNi is shown (Ref. 61). The lattice spacings were taken from the AlNi(110) and $Al_3Ni_2(110)/Al_3Ni_2(102)$ peaks.

An exception to these considerations is AlNi itself [Fig. 1(a)], which has both a high melting point at 1911 K (providing a consistently large driving force for nucleation) and is stable over a wide range of compositions (making nucleation in a composition gradient possible). Since both the liquid phase and cubic AlNi appeared in the same frame (at $t=165$ μs), and given the temporal and spatial resolution of the measurement, we cannot say definitively whether AlNi nucleates in the multilayer (presumably in the Al layers at the Al/Ni interfaces) or precipitates from the liquid. However, from the dynamic TEM experiments it is clear that the liquid always coexists with a solid phase; there is no region in the reaction front that is completely molten.[26] This is consistent with our own data (Fig. 3), in which we see that the peak area for AlNi (once formed) is nearly constant until around the time the maximum temperature is reached, and only increases substantially once cooling begins ($t=4$ ms). Although a dissolution/precipitation mechanism for the formation of AlNi has been predicted for thicker multilayers,[47] in our nanoscale multilayers it seems unlikely that AlNi forms solely by precipitation from the liquid. Instead, there is a more complex partitioning of AlNi and liquid in the advancing reaction front, followed by continued growth of AlNi once the reaction front has passed.

It is interesting to note that while the temperature rises most quickly at short times (<1 ms) when a large amount of mixing is occurring, it continues to rise until $t\approx5$ ms, well after the reaction front has passed. This suggests that intermixing of Al and Ni continues behind the reaction front. The evolution of the lattice parameter of AlNi (Fig. 5) provides additional evidence for this. Between $t=1$ and 5 ms, the lattice parameter of AlNi decreases, even though the temperature is continuing to increase. (At longer times the lattice parameter decreases due to thermal contraction as the foil cools.) We can understand this if we recognize that the AlNi lattice parameter is a function of stoichiometry. Since the atomic volume of Al is greater than that of Ni,[48] we expect that the lattice parameter of AlNi will decrease with increasing Ni content. Therefore, the decrease in lattice parameter with increasing temperature indicates that the AlNi is becoming significantly more Ni-rich. The decrease in lattice parameter with increasing temperature is consistent with an increase in Ni content of the AlNi of approximately 10 at. %.

B. AlNi foils

The sequence of phase formation for the AlNi foils was similar to that for Al_3Ni_2 foils [Fig. 6(a)]. Again, cubic AlNi and an Al-rich liquid phase were the first new phases to form. Because of the higher reaction velocity in this system (Table I), the reaction front arrives at the x-ray beam at approximately $t=130$ μs, so the new phases are apparent in the $t=110$ μs frame.

Cubic AlNi and liquid Al were the only phases present until cubic Al_8V_5 formed and the amorphous phase disappeared some 35 ms after passage of the reaction front [Fig. 6(a)]. AlNi is the only stable phase for foils of this composition at 1073 K (Ref. 49) (the lowest published isothermal section of the ternary phase diagram we have found), but the composition is close to the solvus. Since the general trend is for decreasing solubility of V in AlNi with decreasing temperature, it is possible that at lower temperatures Al_8V_5 might be stable, but this would not explain why we observe its formation at higher temperatures (1240 ± 150 K). A more likely possibility is that Al_8V_5 nucleates from the liquid, since its melting point is rather high (~1670 K). We note, though, that this would require the liquid to be significantly enriched in V.

As with the Al_3Ni_2 multilayers, we observed a different phase formation sequence upon slow heating in the DSC than in the self-propagating reaction. The sequence of phases in the *in situ* x-ray diffraction experiments was

$$\mathrm{Al+Ni\rightarrow AlNi+Al(liquid)\rightarrow AlNi},$$

while for foils heated in the DSC we observed

$$\mathrm{Al+Ni\rightarrow Al+Ni+Al_9Ni_2\rightarrow Ni+Al_3Ni\rightarrow Al_3Ni_2\rightarrow AlNi},$$

neglecting the minor V-containing phases. Again we attribute the difference to the lack of time for nucleation of the intermetallics Al_9Ni_2, Al_3Ni, and Al_3Ni_2 during rapid heating.

Interestingly, in contrast to the behavior in the Al_3Ni_2 multilayers, the lattice parameter of AlNi did not change over the interval 0.5 to 20 ms (Fig. 5). During this time the peak area of AlNi increased slightly, while that of the amorphous phase decreased [Fig. 6(b)]. This suggests that AlNi was growing from the liquid without significant compositional redistribution. [We note that a lack of continued mixing is consistent with the nearly constant temperature over this interval, Fig. 6(b)]. The difference in behavior is likely directly related to the overall composition of the multilayers. With an overall composition that is more Al-rich, the Al_3Ni_2 multilayers produce AlNi that is initially more Al-rich and which then rejects Al into the liquid to satisfy equilibrium

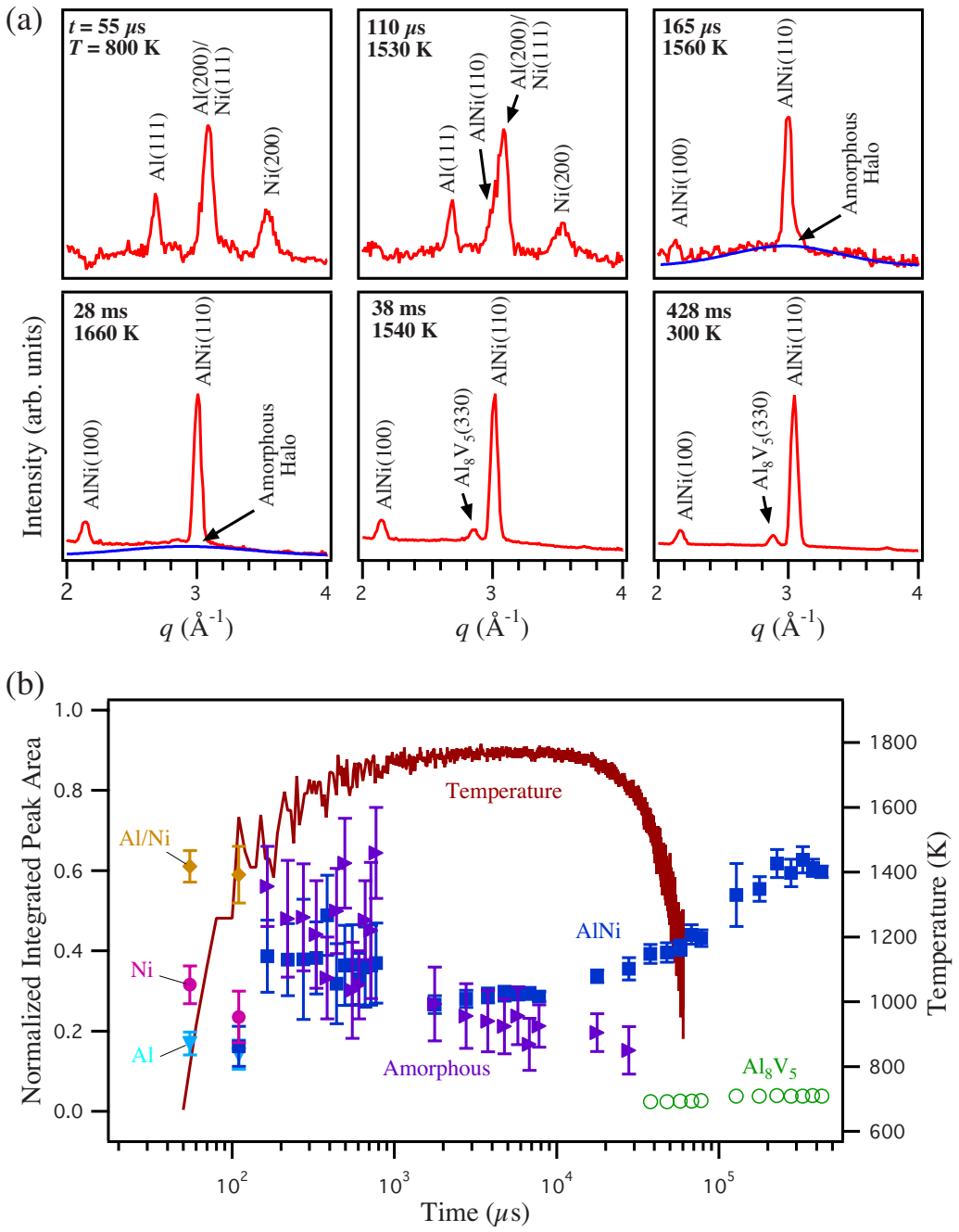

FIG. 6. (Color online) (a) Diffraction patterns of phase transformations during a self-propagating reaction in an AlNi foil. The blue line in patterns at $t = 165$ μs and 28 ms is a fit to the broad halo in the data which is attributed to the presence of an amorphous phase during this time range. (b) The integrated area of the peaks and temperature throughout the reaction, including cooling. Areas labeled "AlNi" were measured from the AlNi(110) peak. (Adapted from Ref. 28.)

conditions. The AlNi multilayer have more Ni in comparison, apparently requiring less compositional redistribution once the AlNi has formed.

C. $Zr_{55}Ni_{45}$ foils

The diffraction patterns observed prior to the arrival of the reaction front at the x-ray beam show several peaks from hcp Zr and a peak from fcc Ni(111) that is rather weak due to crystallographic texture in the vapor-deposited multilayer (Fig. 7). As the reaction front enters the beam (at $t \simeq 1.2$ ms), we observe the development of the orthorhombic intermetallic ZrNi(002) peak as a shoulder on the Zr(101) peak at $q_{max} \simeq 3.0$ Å^{-1}. It is likely that the ZrNi(111) peak was also growing at this time, but it cannot be resolved from the Zr(101) peak with which it overlaps.

We also observed evidence of another crystalline phase at this time, in the form of a small peak at $q \simeq 2.85$ Å^{-1}. This peak could have been from either ZrNiV or ZrV_2, although we cannot determine which because other peaks from these phases either overlap with peaks from the dominant ZrNi phase or are too weak to be observed. Also at this time, there was an increase in the background, which, like the Al/Ni multilayers, we attribute to an amorphous phase. By the next frame (0.3 ms later, at $t = 1.5$ ms) the reaction front has com-

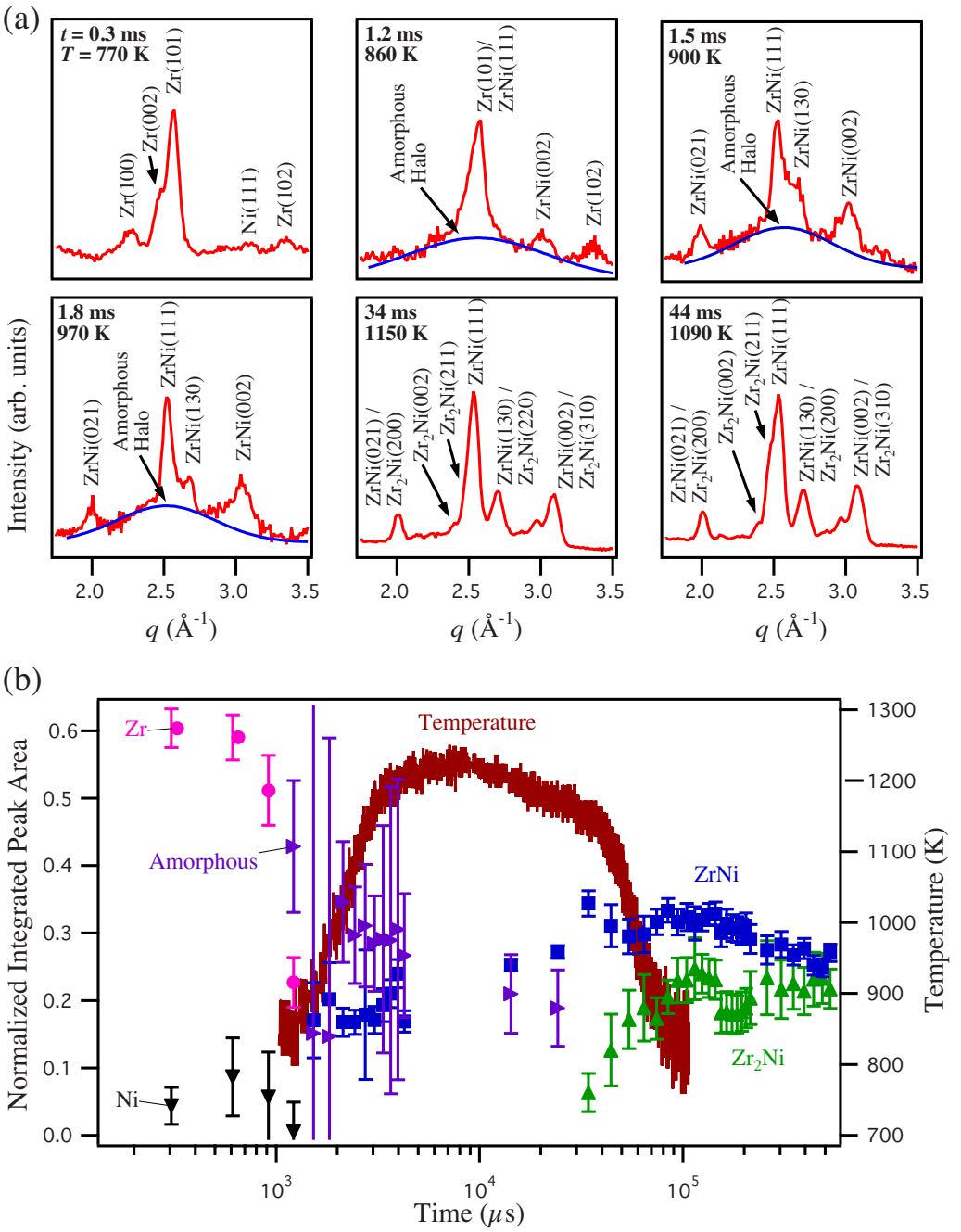

FIG. 7. (Color online) (a) Diffraction patterns of phase transformations during a self-propagating reaction in a Zr_2Ni foil. The blue line in patterns at t = 1.2, 1.5, and 1.8 ms is a fit to the broad halo in the data which is attributed to the presence of an amorphous phase during this time range. (b) The integrated area of the peaks and temperature throughout the reaction, including cooling. Areas labeled "ZrNi" and "Zr_2Ni" were measured from the ZrNi(111) and Zr_2Ni(211) peaks, respectively.

pletely passed the x-ray beam and the only phases present are ZrNi and the amorphous phase (hcp Zr and fcc Ni having been completely consumed). Similar to the reactions in the Al/Ni multilayers, the amorphous phase disappeared during cooling (~34 ms) and tetragonal Zr_2Ni formed [Fig. 7(a)]. An inflection point indicative of an exothermic reaction in the temperature profile was also observed at this time [Fig. 7(b)], also suggesting the nucleation and growth of a solid (presumably Zr_2Ni) from a liquid. The final microstructure consists of Zr_2Ni and ZrNi, which are the equilibrium phases at room temperature for a binary alloy with the composition $Zr_{55}Ni_{45}$.[49]

In the Al/Ni multilayers, the presence of an amorphous phase is not surprising, since the temperature of the reaction front exceeds the melting point of the Al layers. In the Zr/Ni system, however, the lowest temperature at which a liquid is stable is ~1230 K [Fig. 1(b)], higher than both the observed maximum temperature of the reaction front (1200 ± 150 K) and the calculated adiabatic reaction temperature (1225 K).[9] (This is based on the binary Zr–Ni phase diagram; we are unaware of any published data on the Zr–Ni–V system at the compositions of interest.) Furthermore, even if the heat of reaction was sufficient to raise the temperature to the

liquidus, additional heat (the enthalpy of fusion) would be required for melting to occur.

It is, therefore, unlikely that the amorphous phase we observe is due to melting of either the Ni or Zr layers. Instead, we propose that is it the result of a solid-state amorphization reaction, which is known to occur in Ni/Zr multilayers.[14,50] In this picture, the first phase to form at the Ni/Zr interfaces is an amorphous solid produced by rapid diffusion of Ni into Zr (since Ni is known to diffuse more rapidly into Zr than vice versa[51]). The position of the amorphous peak ($q_{max} \simeq 2.5-2.6$ Å^{-1} seen in Fig. 7) suggests that the amorphous alloy is ~75 at. % Zr,[52,53] consistent with the idea that it forms by diffusion of Ni into the Zr layers. It is interesting to note that this composition is also approximately the minimum concentration of Ni necessary for formation of an amorphous phase according to the Egami instability criterion.[54]

Once the amorphous interfacial layer forms, the temperature of the material in the reaction front quickly exceeds the glass transition temperature of the amorphous alloy, producing a liquid and facilitating additional rapid intermixing of the elemental constituents. At the heating rates typical of differential scanning calorimetry (~1 K s^{-1}) the glass transition temperature T_g is 600–900 K for Zr–Ni amorphous alloys, with Zr-rich alloys being at the lower end of this range.[55,56] Since amorphous phase formation is driven by diffusion of Ni into Zr, we assume that the amorphous phase in the self-propagating reactions is initially Zr-rich and therefore has $T_g \approx 600$ K. The glass transition temperature of amorphous alloys does increase with heating rate; and in our experiments the heating rate (Table I) is some five orders of magnitude greater than that of typical calorimetry experiments (~1 K s^{-1}). Assuming a logarithmic dependence of glass transition temperature on heating rate,[57] however, it is likely that the rapid heating in our experiments only raises T_g by ~100 K. Therefore, $T_g \approx 700$ K would appear to be a reasonable estimate for the Zr-rich amorphous phase in Ni–Zr under these conditions. From Fig. 7, we see that this temperature is exceeded very early on in the reaction, so any amorphous phase that forms almost certainly becomes liquid very rapidly.

It is worth noting that apparently neither of the elemental reactants melts during self-propagating reactions in our Zr/Ni multilayers. This indicates that melting of the reactants is not required to sustain a self-propagating reaction. However, we note that intermixing in the solid-state leading to the formation of an amorphous solid and ultimately a supercooled liquid (due to continued heating) would facilitate rapid interdiffusion of the elemental constituents. In contrast to systems where one of the parent phases melts, in Zr/Ni multilayers it appears that the formation of a liquid product enables the self-propagating exothermic reaction to be sustained.

Another difference for the Zr/Ni foils (in comparison to the Al/Ni system), is that the phases formed during slower heating in the DSC are the same as those observed during rapid heating in the *in situ* experiments. However, we cannot determine conclusively whether the sequence of phase formation is the same. At the low heating rates of the DSC, an amorphous phase forms first by solid-state reaction, followed later by nucleation and growth of crystalline ZrNi, as is well known.[14,15] Under rapid heating we observe formation of an amorphous phase and ZrNi apparently simultaneously, but this may reflect the limitations of the *in situ* experiments (in terms of both temporal and spatial resolution and the ability to detect a small amount of an amorphous phase) rather than a true difference in behavior. We note that in the Zr–Ni system, solid-state amorphization is facilitated by a large difference in atomic size and strongly asymmetric atomic diffusion.[50] In contrast, solid-state amorphization is not necessarily expected in Al/Ni multilayers and has never (to our knowledge) been observed.

The final microstructure of the Zr/Ni foils after the self-propagating reaction has a much finer scale than either of the Al/Ni compositions (Fig. 4). This is most likely a consequence of the lower reaction temperature which results in higher nucleation rates and lower growth rates. The microstructure also exhibits a banded structure with regions of smaller grains [Fig. 4(e)], which is not observed in the microstructure produced at slower heating rates in the DSC [Fig. 4(f)]. We have observed similar banded microstructures in other reactive foils, and previously attributed them to non-steady propagation of the reaction front.[37] In particular, one can attribute the regions of large grain size to sudden spikes in the reaction temperature (which result in lower nucleation and higher growth rates), the occurrence of which had been previously predicted from simulations of the propagating reaction.[58] An alternative explanation—which we now consider more likely—is that the banded microstructure results from transverse propagation of the reaction front in a stepwise fashion, as has recently been observed in Co/Al multilayers.[59] Because the periodicity of the microstructure is smaller than the spatial resolution of our *in situ* measurement, we are unable to investigate this in detail. However, we believe that this uncertainty regarding the origin of the banded microstructure probably does not influence the observed phase formation sequence. This conclusion is based on the observation of the same final phases in both the fine-grained and coarse-grained regions as well as the observation that the phase formation sequence is the same for the self-propagating reactions and the reaction at slow (DSC) heating rates.

The discussion above does not take into account the possibility that the presence of V may influence the sequence of phase formation (other than the obvious formation of V-containing phases as predicted by the respective ternary phase diagrams) in self-propagating reactions. However, we note that in reactions observed under slow heating (such as in the DSC) similar results are obtained in multilayers with and without vanadium. Furthermore, the amount of V in our multilayers (≤4 at. %) is small and is well below the limit for solid solubility of V in Ni (≥12 at. %). For these reasons, we do not expect that the presence of V has a significant effect on the general sequences of phase formation described above.

V. CONCLUSIONS

Self-propagating reactions in nanostructured multilayer foils provide a scientific opportunity to study intermetallic

phase formation at rapid heating rates (10^6–10^7 K s^{-1}) in a laboratory setting. To achieve the necessary spatial and temporal resolution to observe such transformations, we used synchrotron x-ray focused to a small spot (60 μm diameter) and a fast PAD with microsecond temporal resolution. In this study, we examined two different compositions of Al–Ni foils (nominally AlNi and Al_3Ni_2 in overall composition) and a Zr–Ni foil with overall composition of nominally $Zr_{55}Ni_{45}$.

The phase sequences in the AlNi and Al_3Ni_2 foils were identical, except for the final phases that formed during cooling. In both compositions the first phases to form were an Al-rich liquid and the cubic intermetallic AlNi (which likely formed by nucleation from the liquid). This is different from the transformations that occur in identical foils under slow heating ($\sim 10^{-1}$ K s^{-1}), where we observed the formation of crystalline Al_9Ni_2 first, and no liquid phase.

In the $Zr_{55}Ni_{45}$ foils, however, the same phases form during self-propagating and slow heating reactions. In both cases we observe formation of an amorphous Zr–Ni phase and crystalline ZrNi. During slow heating, the amorphous phase forms first by a solid-state reaction, followed by nucleation and growth of the crystalline intermetallic. Under rapid heating, we observe formation of the amorphous and crystalline phases simultaneously, but this may be due to the limited temporal and spatial resolution of the *in situ* experiments. In the self-propagating reactions, the temperature of the reaction front never reaches the lowest-lying liquidus on the Zr–Ni phase diagram. This implies that in contrast to the Al–Ni case, the formation of the amorphous phase does not occur by melting of a crystalline phase. Instead, we believe that a Zr-rich amorphous solid formed as a result of a solid-state amorphization reaction, similar to that observed during slow heating. After formation of the solid amorphous phase, the temperature continues to rise, ultimately exceeding the glass transition temperature and thus leading to the formation of a supercooled liquid. We note that this transformation would facilitate rapid interdiffusion, potentially enabling the self-propagation of the exothermic reaction front.

ACKNOWLEDGMENTS

We gratefully acknowledge Alexander Kazimirov, Darol Chamberlain, Daniel Schuette, Darren Southworth, and Harish Nathani for their assistance with the x-ray experiments; Sterling Cornaby and Don Bilderback for providing the x-ray capillary; Mark Koontz for his assistance with the scanning electron microscopy; and Sean Brennan for peak-fitting routines used in data analysis. Financial support for this work is provided by the National Science Foundation under Grant No. DMI-0300396 (JCT, TPW, TCH), with Howmet Research Corporation as our industrial partner; the Office of Naval Research under Grant No. N00014-07-1-0740 (NW, TPW, TCH); and the Department of Energy under Grant No. FG02-97ER62443 (LJK, MWT, SMG). Portions of this research were conducted at the Cornell High Energy Synchrotron Source (CHESS), which is supported by the National Science Foundation and the National Institutes of Health/National Institute of General Medical Sciences under Grant No. DMR-0225180. The views expressed are those of the authors, and not necessarily those of the supporting agencies.

[1] C. Michaelsen, K. Barmak, and T. P. Weihs, J. Phys. D **30**, 3167 (1997).
[2] J. A. Floro, J. Vac. Sci. Technol. A **4**, 631 (1986).
[3] C. E. Wickersham, Jr. and J. E. Poole, J. Vac. Sci. Technol. A **6**, 1699 (1988).
[4] L. A. Clevenger, C. V. Thompson, R. C. Cammarata, and K. N. Tu, Appl. Phys. Lett. **52**, 795 (1988).
[5] L. A. Clevenger, C. V. Thompson, and K. N. Tu, J. Appl. Phys. **67**, 2894 (1990).
[6] E. Ma, C. V. Thompson, L. A. Clevenger, and K. N. Tu, Appl. Phys. Lett. **57**, 1262 (1990).
[7] T. S. Dyer, Z. A. Munir, and V. Ruth, Scr. Mater. **30**, 1281 (1994).
[8] T. P. Weihs, A. Gavens, M. E. Reiss, D. V. Heerden, A. Draffin, and D. Stanfield, Proceedings of TMS, Orlando, FL, 1997.
[9] A. J. Gavens, D. V. Heerden, A. B. Mann, M. E. Reiss, and T. P. Weihs, J. Appl. Phys. **87**, 1255 (2000).
[10] T. Barbee and T. Weihs, U.S. Patent No. 5,547,715 (1996).
[11] J. C. Trenkle, L. J. Koerner, M. W. Tate, S. M. Gruner, T. P. Weihs, and T. C. Hufnagel, Appl. Phys. Lett. **93**, 081903 (2008).
[12] U. Gösele and K. N. Tu, J. Appl. Phys. **53**, 3252 (1982).
[13] C. V. Thompson, J. Mater. Res. **7**, 367 (1992).
[14] B. M. Clemens, Phys. Rev. B **33**, 7615 (1986).
[15] B. M. Clemens, W. L. Johnson, and R. B. Schwarz, J. Non-Cryst. Solids **61-62**, 817 (1984).
[16] W. J. Meng, C. W. Nieh, E. Ma, B. Fultz, and W. L. Johnson, Mater. Sci. Technol. **97**, 87 (1987).
[17] P. J. Desré and A. R. Yavari, Phys. Rev. Lett. **64**, 1533 (1990).
[18] P. J. Desré, Acta Metall. Mater. **39**, 2309 (1991).
[19] F. Hodaj and P. J. Desré, Acta Mater. **44**, 4485 (1996).
[20] F. Hodaj and A. M. Gusak, Acta Mater. **52**, 4305 (2004).
[21] A. M. Gusak, F. Hodaj, and A. O. Bogatyrev, J. Phys.: Condens. Matter **13**, 2767 (2001).
[22] M. H. da Silva Bassani, J. H. Perepezko, A. S. Edelstein, and R. K. Everett, Scr. Mater. **37**, 227 (1997).
[23] K. J. Blobaum, D. V. Heerden, A. J. Gavens, and T. P. Weihs, Acta Mater. **51**, 3871 (2003).
[24] V. V. Boldyrev, V. V. Alexandrov, M. A. Korchagin, B. P. Tolochko, S. N. Gusenko, A. S. Sokolov, M. A. Sheromov, and N. Z. Liakhov, Dokl. Akad. Nauk SSSR **259**, 1127 (1981).
[25] J. Wong, E. M. Larson, J. B. Holt, P. A. Waide, B. Rupp, and R. Frahm, Science **249**, 1406 (1990).
[26] J. S. Kim, T. LaGrange, B. W. Reed, M. L. Taheri, M. R. Armstrong, W. E. King, N. D. Browning, and G. H. Campbell, Science **321**, 1472 (2008).
[27] B. Müller and U. Renz, Rev. Sci. Instrum. **72**, 72 (2001).
[28] J. C. Trenkle, T. P. Weihs, T. C. Hufnagel, L. J. Koerner, M. W. Tate, and S. M. Gruner, Proceedings of JANNAF, 2008.
[29] A. Kazimirov, D. M. Smilgies, Q. Shen, X. H. Xiao, Q. Hao, E. Fontes, D. H. Bilderback, S. M. Gruner, Y. Platonov, and V. V. Martynov, J. Synchrotron Radiat. **13**, 204 (2006).
[30] R. Huang and D. Bilderback, J. Synchrotron Radiat. **13**, 74 (2006).
[31] G. Rossi, M. Renzi, E. F. Eikenberry, M. W. Tate, D. Bilderback, E. Fontes, R. Wixted, S. Barna, and S. M. Gruner, J. Synchrotron Radiat. **6**, 1096 (1999).
[32] M. Maret, T. Pomme, A. Pasturel, and P. Chieux, Phys. Rev. B **42**, 1598 (1990).
[33] G. W. Lee, A. K. Gangopadhyay, K. F. Kelton, R. W. Hyers, T. J. Rathz, J. R. Rogers, and D. S. Robinson, Phys. Rev. Lett. **93**, 037802 (2004).
[34] S. K. Das, J. Horbach, M. M. Koza, S. M. Chatoth, and A. Meyer, Appl. Phys. Lett. **86**, 011918 (2005).
[35] J. Brillo, A. Bytchkov, I. Egry, L. Hennet, G. Mathiak, I. Pozdnyakova, D. L. Price, D. Thiaudiere, and D. Zanghi, J. Non-Cryst. Solids **352**, 4008 (2006).
[36] *Handbook of Ternary Alloy Phase Diagrams*, edited by P. Villars, A. Prince, and H. Okamoto (ASM International, Materials Park, Ohio, 1995).
[37] J. C. Trenkle, J. Wang, T. P. Weihs, and T. C. Hufnagel, Appl. Phys. Lett. **87**, 153108 (2005).
[38] A. S. Edelstein, R. K. Everett, G. Y. Richardson, S. B. Qadri, E. I. Altman, J. C. Foley, and J. H. Perepezko, J. Appl. Phys. **76**, 7850 (1994).
[39] U. Rothhaar, H. Oechsner, M. Scheib, and R. Müller, Phys. Rev. B **61**, 974 (2000).
[40] C. Michaelsen, G. Lucadamo, and K. Barmak, J. Appl. Phys. **80**, 6689 (1996).

[41]T. S. Dyer and Z. A. Munir, Metall. Mater. Trans. B **26**, 603 (1995).
[42]A. Zalar, S. Hofmann, D. Kohl, and P. Panjan, Thin Solid Films **270**, 341 (1995).
[43]F. Chevrier, A. Delobbe, A. Traverse, and D. Zanghi, J. Appl. Phys. **90**, 2718 (2001).
[44]P. Bhattacharya, S. Bysakh, K. N. Ishihara, and K. Chattopadhyay, Scr. Mater. **44**, 1831 (2001).
[45]E. Ma, C. V. Thompson, and L. A. Clevenger, J. Appl. Phys. **69**, 2211 (1991).
[46]K. Barmak, C. Michaelsen, and G. Lucadamo, J. Mater. Res. **12**, 133 (1997).
[47]A. S. Shteinberg, V. A. Shcherbakov, and Z. A. Munir, Combust. Sci. Technol. **169**, 1 (2001).
[48]*Smithells Metals Reference Book*, edited by W. F. Gale and T. C. Totemeir (ASM International, Materials Park, Ohio, 1997).
[49]J. C. Schuster, *HF-N-Si Phase Diagram*, edited by P. Villars, H. Okamoto, and K. Cenzual (ASM International, Materials Park, Ohio, 2006).
[50]W. L. Johnson, Prog. Mater. Sci. **30**, 81 (1986).
[51]Y. T. Cheng, W. L. Johnson, and M. A. Nicolet, Appl. Phys. Lett. **47**, 800 (1985).
[52]T. Aihara, Jr., Y. Kawazoe, and T. Masmoto, J. Non-Cryst. Solids **205-207**, 875 (1996).
[53]Y. D. Dong, G. Gregan, and M. G. Scott, J. Non-Cryst. Solids **43**, 403 (1981).
[54]T. Egami and Y. Waseda, J. Non-Cryst. Solids **64**, 113 (1984).
[55]A. L. Greer, Science **267**, 1947 (1995).
[56]Z. Altounian, G. H. Tu, and J. O. Strom-Olsen, J. Appl. Phys. **54**, 3111 (1983).
[57]M. Lasocka, Mater. Sci. Eng. **23**, 173 (1976).
[58]S. Jayaraman, O. M. Knio, A. B. Mann, and T. P. Weihs, J. Appl. Phys. **86**, 800 (1999).
[59]J. P. McDonald, V. C. Hodges, E. D. Jones, and D. P. Adams, Appl. Phys. Lett. **94**, 034102 (2009).
[60]Reprinted with permission of ASM International®. All rights reserved. www.asminternational.org
[61]*Thermal Expansion: Metallic Elements and Alloys*, edited by Y. S. Touloukian (IFI/Plenum, New York, 1975).